Research Square

Preprints are preliminary reports that have not undergone peer review.
They should not be considered conclusive, used to inform clinical practice,
or referenced by the media as validated information.

Exact certification of irrational global minimizers from inexact sum-of-squares certificates

Katherine Xie

kathex5@uci.edu

University of California, Irvine

Research Article

Keywords: symbolic-numeric computation; exact certification; sums of squares; rational certificates; semidefinite programming; Bernstein basis; interval arithmetic; Kronecker substitution; formal verification; Lean; Thomson problem; Coulomb energy

Posted Date: November 19th, 2026

DOI: https://doi.org/10.21203/rs.3.rs-11723965/v1

License: This work is licensed under a Creative Commons Attribution 4.0 International License.
Read Full License

Additional Declarations: The authors declare no competing interests.

EXACT CERTIFICATION OF IRRATIONAL GLOBAL MINIMIZERS FROM INEXACT SUM-OF-SQUARES CERTIFICATES

KATHERINE XIE

Abstract. Sum-of-squares programming can certify polynomial inequalities, but in practice its certificates are computed numerically, in floating-point arithmetic. A common way to make them exact is to round them to rational numbers, which typically needs some slack. Bounds that certify optimality at an irrational minimizer have essentially no slack, so rounding alone is generally not enough. We describe one way to handle this case and apply it to the Thomson problem: placing N equal charges on the unit sphere to minimize their Coulomb energy. We round a numerical three-point semidefinite certificate and keep the rounding error as an explicit residual, which gives an energy bound within 10^{-50} of the candidate configuration. A quantitative form of complementary slackness, a finite case analysis and a local Hessian bound are then used to turn this nearly tight bound into an exact result. In this way we obtain a computer-assisted proof that the tricapped trigonal prism ($N = 9$) and the capped square antiprism ($N = 10$) are the unique minimizers up to rotations, reflections and relabeling. Both results are also formalized in the Lean 4 proof assistant.

1. Introduction

1.1. **Rational certificates for tight bounds.** Hybrid symbolic-numeric methods are the standard way to obtain exact lower bounds in polynomial optimization. A semidefinite solver computes an approximate sum-of-squares decomposition, which is then converted into an identity with rational coefficients and verified in exact arithmetic [19, 15, 20, 13, 16]. The resulting certificate can be checked independently of the solver, and also inside a proof assistant [10]. The conversion step relies on slack. If the numerical Gram matrix is positive definite with a margin larger than the rounding error, one can round it and project it onto the affine space of matrices that satisfy the identity exactly, and the result is still positive semidefinite [20].

Tight bounds have no such slack, and in extremal geometry the tight bounds are the ones of interest: they show that a specific configuration is optimal. By complementary slackness, an exactly tight certificate must vanish at the optimal solution. If the optimal solution is irrational, a rational certificate generally cannot do this, and the numerical certificate lies on the boundary of the cone, where rounding destroys positivity. In the problem studied here the objective is, moreover, not a polynomial. Exact rounding is therefore not an option.

1.2. **Approach: an explicit residual in place of exactness.** Our approach is to give up exactness of the certificate itself. We accept a small, explicitly bounded error and recover an exact statement afterwards, in four steps.

(1) *Rounding with a residual.* The numerical factors of the semidefinite blocks and of the weighted sums of squares are rounded to rational columns. Positivity then holds by construction, since every block has the form CC^T with C rational. The certificate identity holds exactly with an extra term, a residual polynomial R with rational coefficients. The residual has no prescribed sign, and only the exact ℓ^1-norm ρ of its coefficients enters the

Date: 12 November 2026.

2020 *Mathematics Subject Classification.* Primary 68W30; Secondary 90C22, 90C23, 90C26, 65G30, 68V15, 52C17.

Key words and phrases. Symbolic-numeric computation, exact certification, sums of squares, rational certificates, semidefinite programming, Bernstein basis, interval arithmetic, Kronecker substitution, formal verification, Lean, Thomson problem, Coulomb energy.

argument, so neither a projection nor an interior margin is needed. The bound is within a known multiple of ρ of the optimum, here less than 10^{-50}.

(2) *Quantitative complementary slackness.* Exact complementary slackness would force every pair statistic of an optimal solution into the contact set of the certificate. A quadratic lower bound for the interpolation gap, obtained from Hermite's remainder formula, converts the small duality gap into an explicit proximity radius δ to the contact set.

(3) *Combinatorial recovery.* The relaxation discards a rank constraint. Reimposing it, an exhaustive enumeration over determinant conditions, made rigorous by perturbation bounds, shows that the approximate pair values admit only one consistent labeling. The enumeration is an outer approximation: a case is discarded only when an enclosure is separated from zero.

(4) *A local certificate on an explicit radius.* After the symmetry is removed, a validated lower bound for the Hessian holds on a box whose radius exceeds the localization error. This excludes every other minimizer near the conjectured one.

Each step produces an explicit constant that the next one uses, and the argument closes when these constants are compatible. Section 2 states the method as a procedure with its acceptance tests, and Table 1 gives the values that occur.

1.3. **Application: the Thomson problem.** For N points on the unit sphere $\mathbb{S}^2 = \{x \in \mathbb{R}^3 : \|x\| = 1\}$ consider

$$\min_{X \in (\mathbb{S}^2)^N} E_N(X), \qquad E_N(X) = \sum_{0 \le i < j < N} \frac{1}{\|x_i - x_j\|}, \qquad X = (x_0, \dots, x_{N-1}). \tag{1}$$

This is the Coulomb energy of N equal point charges, and (1) is known as the Thomson problem [23]. It is nonconvex, singular at collisions, and invariant under the group $O(3) \times S_N$ of orthogonal transformations and relabelings, so minimizers are at best unique up to this action. It is a standard test case for global optimization heuristics: basin-hopping [27] produces putative minimizers for hundreds of points [28], but a numerical search does not certify that no better configuration exists. For unit vectors $\|x - y\|^2 = 2 - 2x \cdot y$, so, writing $t_{ij} = x_i \cdot x_j$,

$$\phi(t) = (2 - 2t)^{-1/2}, \qquad E_N(X) = \sum_{i<j} \phi(t_{ij}). \tag{2}$$

The objective is a separable non-polynomial function of the Gram matrix $G = (t_{ij})$. The Gram matrices of configurations are exactly the positive semidefinite matrices with unit diagonal and rank at most three. Dropping the rank constraint and imposing positivity conditions on two- and three-point statistics gives the linear programming bounds of Delsarte type [7, 31] and the three-point semidefinite bounds of Bachoc–Vallentin and Cohn–Woo [2, 4]. Our certificates are rational dual solutions of such relaxations.

For nine points the candidate is a *tricapped trigonal prism*: two aligned equilateral triangles at opposite heights, together with three equatorial caps facing the rectangular sides of the prism. For ten points it is a *capped square antiprism*: two antipodal poles and two parallel squares at opposite heights, rotated through $\pi/4$ relative to each other. Each candidate belongs to a one-parameter family whose energy has a unique critical point, at an irrational parameter enclosed in an explicit rational bracket (Section 3). We write P_N^* for the optimized configuration and $E_N^* = E_N(P_N^*)$.

Theorem 1.1. *Let $N \in \{9, 10\}$. Every configuration X of N distinct points on $\mathbb{S}^2$ satisfies $E_N(X) \ge E_N^*$. Equality holds if and only if there are $Q \in O(3)$ and a permutation π of $\{0, \dots, N-1\}$ such that*

$$x_i = Q p_{\pi(i)} \quad (0 \le i < N), \qquad P_N^* = (p_0, \dots, p_{N-1}).$$

Configurations related in this way are called *congruent*. No symmetry is assumed of a competing configuration.

1.4. **Contributions.** The contributions of this paper are the following.

- *Certification without exact tightness.* We describe how an inexact rational sum-of-squares certificate, whose residual is kept explicitly and bounded only through its coefficient norm, can prove exact optimality and uniqueness of an irrational minimizer. The extra ingredients are a coercivity estimate, a combinatorial recovery step and a local certificate on an explicit radius (Section 2).
- *A reduction to finite checks.* All statements about the infinitely many configurations reduce to exact polynomial identities over $\mathbb{Q}$ (the largest is trivariate of degree 20, from certificates of about 10 MB), Bernstein-basis inequalities on rational cells, interval enclosures over the parameter brackets, and one finite classification. Section 10 gives the algorithms and their sizes.
- *Computer-assisted proofs for $N = 9$ and $N = 10$.* The procedure proves Theorem 1.1 for $N = 9$ and $N = 10$. The certificates and their checkers are archived [29, 30].
- *Kernel-checked certificates in a proof assistant.* Both theorems are formalized in Lean 4 with Mathlib [6, 22], and the formal proofs depend only on the standard axioms. Every finite certificate used in the formal proofs is checked by the Lean kernel, without trusted native code. To make this feasible we use integer-scaled explicit formulas, a zero test by Kronecker substitution [26, 11] with proved coefficient and degree bounds, and packed sign tests for positivity on boxes (Section 10.6).

The certificates were found by numerical semidefinite optimization, but only their exact rational forms enter the proof. The analytic reductions (kernel positivity, the interpolation remainder, the perturbation bounds, the alignment estimate and the Taylor argument) are proved in full in this paper.

1.5. **Related work.** *Exact certificates from numerical solutions.* Sums of squares and moment hierarchies for polynomial optimization go back to Parrilo [19] and Lasserre [15]. Peyrl and Parrilo round and project strictly feasible numerical solutions to exact rational decompositions [20]. Kaltofen, Li, Yang and Zhi certify the global optimality of approximate polynomial factorizations in exact arithmetic by rationalizing sums of squares with floating-point scalars [13]. Magron and Safey El Din compute exact decompositions for several classes of positive polynomials, including Putinar representations on compact semialgebraic sets [16]. These methods need strict feasibility. Our setting has no interior margin, and the residual is bounded instead of eliminated.

Validated numerics and formal verification. Rigorous global optimization by interval methods is surveyed in [18], and we use Arb ball arithmetic [12]. The Bernstein basis [8] gives range bounds for polynomials on boxes, and Bernstein-based global optimization has been formalized in PVS [17]. Harrison verified nonlinear real inequalities in HOL Light from sum-of-squares certificates [10]. The formal proof of the Kepler conjecture is a landmark computer-assisted optimality proof [9]. Kronecker substitution is a classical device for reducing polynomial arithmetic to integer arithmetic [26, 11]. We use it as a zero test whose injectivity is proved inside the kernel.

Energy minimization on the sphere. Polynomial bounds for spherical codes and designs go back to Delsarte, Goethals and Seidel [7]. Yudin bounded potential energies from below by positive expansions in orthogonal polynomials [31], and Andreev used this method for the icosahedron [1]. Cohn and Kumar showed that many symmetric configurations are universally optimal [3]; for these the linear programming bound is exactly tight. Semidefinite three-point bounds are due to Bachoc and Vallentin [2] and, for energy, to Cohn and Woo [4]. De Laat constructed convergent moment hierarchies for energy problems [5]. Schwartz proved optimality and uniqueness for five points by a computer-assisted geometric argument [21]. Kryvonos, Liehr and Taylor proved optimality and uniqueness of the square antiprism for eight points [14]. Related Lean developments exist for eight points [25] and for seven points [24].

1.6. **Organization.** Section 2 states the certification procedure and its acceptance tests. Sections 3–9 carry it out for the two candidates: the candidate families (Section 3), the positive kernels (Section 4), the domain reduction (Section 5), the rational certificate with residual (Section 6), quantitative complementary slackness (Section 7), combinatorial recovery (Section 8) and the local certificate (Section 9), which completes the proof of Theorem 1.1. Section 10 describes the verification algorithms, the certificate sizes and the Lean formalization. Section 11 discusses the scope of the method. The appendices collect the parameter enclosures, the certificate data, the alignment estimate, the Hessian calculation and the addition theorem.

2. The certification procedure

We now state the method as a procedure. Its input is numerical data; its output, when all checks succeed, is a proof consisting of finitely many exact or validated checks together with the analytic lemmas of Sections 4–9. Call a configuration X *competitive* if $E_N(X) \le E_N^*$. Theorem 1.1 is equivalent to the statement that every competitive configuration is congruent to P_N^*. The candidate has a finite set $\mathcal{A}_N$ of pairwise inner products, the *target set*: six values for the prism and seven for the antiprism.

Procedure 2.1 (Certifying an irrational minimizer up to symmetry)**.** *Input:* a one-parameter candidate family; numerical solutions of a two-point linear program and of a three-point semidefinite program; a coercivity constant γ, a local radius s and a Hessian margin λ.

(0) *Candidate.* Enclose the unique critical parameter of the family in a rational bracket. Every later quantity that depends on the parameter is enclosed uniformly over this bracket. (Section 3; interval arithmetic.)

(1) *Domain reduction.* Certify a separation bound b: every competitive configuration has $t_{ij} < b$ for $i \neq j$. Every triple then lies in $D_b = [-1, b]^3 \cap \{\Delta \ge 0\}$, and $b - u$ becomes available as a multiplier. (Section 5; Bernstein bounds.)

(2) *Rounded dual certificate.* Choose a rational polynomial m below the averaged Hermite minorant and a rational energy bound $U > E_N^*$. Round the numerical factors of the three-point certificate on D_b to rational columns. Define the residual R as the exact difference between the two sides of the certificate identity, and compute $\rho = \|R\|_1$, the sum of the absolute values of its coefficients. (Section 6; exact arithmetic over $\mathbb{Q}$.)

(3) *Localization.* With $C = \binom{N}{2}$, choose $\delta > 0$ such that

$$2C\rho < \gamma\,\delta^2. \tag{3}$$

Certify $\phi - H \ge \gamma\,\mathrm{dist}(\cdot, \mathcal{A}_N)^2$ on $[-1, b]$ for the Hermite interpolant H of the certificate. Then every competitive pair value lies within δ of $\mathcal{A}_N$. (Section 7; interval arithmetic.)

(4) *Combinatorial recovery.* Choose a classification radius $\eta \ge \delta$ and run the exhaustive anchor enumeration of Section 8. Accept if every surviving clique is isomorphic to the labeled Gram matrix of the candidate. (Exact determinant polynomials with interval enclosures.)

(5) *Local certificate.* Certify $D^2 E_N \succeq \lambda I$ on the box $\|q\|_\infty \le s$ in slice coordinates, uniformly over the bracket, and check

$$128\,\delta < s, \qquad \delta \le 10^{-9}. \tag{4}$$

(Section 9; ball arithmetic.)

Output: a proof of Theorem 1.1 for this N if every check succeeds, and failure otherwise.

The factor 128 and the condition $\delta \le 10^{-9}$ come from the alignment estimate (Lemma 9.1). Steps 3 and 5 interact through the two radii. The global certificate determines δ, the local certificate determines s, and the argument closes only if $128\delta < s$. Table 1 gives the values used.

TABLE 1. The quantities computed by Procedure 2.1. In both cases the Hessian in slice coordinates is bounded below by $\lambda = 1/1000$, and the coercivity constant is $\gamma = 10^{-12}$.

Step	Quantity	Tricapped trigonal prism	Capped square antiprism
	Number of points N	9	10
	Number of pairs $C_N = \binom{N}{2}$	36	45
1	Separation cutoff b_N	567/1000	23/50
2	Residual budget $2C_N\rho_N$	$< 10^{-50}$	$< 7.21 \times 10^{-57}$
3	Localization radius δ_N	10^{-19}	10^{-22}
4	Classification radius η_N	10^{-9}	10^{-5}
5	Free local coordinates $2N-3$	15	17
5	Local box radius s_N	10^{-7}	10^{-6}

Both tests pass, and $\delta_N < \eta_N$:

(3): $72\rho_9 < 10^{-50} = 10^{-12}\delta_9^2$, $90\rho_{10} < 7.21 \times 10^{-57} < 10^{-56} = 10^{-12}\delta_{10}^2$,

(4): $128\delta_9 = 1.28 \times 10^{-17} < 10^{-7}$, $128\delta_{10} = 1.28 \times 10^{-20} < 10^{-6}$.

TABLE 2. The finite checks of Procedure 2.1, by step. "Exact" means arithmetic in $\mathbb{Z}$ or $\mathbb{Q}$; "validated" means outward-rounded interval or ball arithmetic.

Step	Finite statement	Method
0	Signs of F' at the bracket endpoints	validated
1	Scalar polynomial inequalities on intervals	exact Bernstein
1	Three-point inequality on boxes ($N = 10$)	validated Bernstein
2	Identity (18) in $\mathbb{Q}[u, v, t]$ and the value of ρ_N	exact
2	$m_N \le M_N$ and $U_N > E_N^*$ over the bracket	validated
3	Lower bounds for the interpolation gap on cells	validated
4	Determinant tests of the classification	exact polynomials, validated signs
5	Hessian lower bound on the box	validated (two implementations)

Table 2 lists the finite checks behind each step; Section 10 describes the algorithms that perform them.

3. THE TWO CANDIDATE FAMILIES

Within a subsection devoted to one value of N, and in the corresponding appendix, we abbreviate E_N by E and suppress the subscript N on P_N^*, E_N^*, $\mathcal{A}_N$ and b_N. The symbol F denotes the energy along the family under consideration. Points are indexed from 0.

3.1. The tricapped trigonal prism.

For $0 < r < 1$, put $h = \sqrt{1 - r^2}$ and define

$$\begin{aligned} p_j(r) &= (r\cos(2\pi j/3), r\sin(2\pi j/3), h), && 0 \le j \le 2, \\ p_{j+3}(r) &= (r\cos(2\pi j/3), r\sin(2\pi j/3), -h), && 0 \le j \le 2, \\ p_{j+6}(r) &= (\cos(\pi/3 + 2\pi j/3), \sin(\pi/3 + 2\pi j/3), 0), && 0 \le j \le 2. \end{aligned}$$

Write $P(r) = (p_0(r), \dots, p_8(r))$ and $F(r) = E(P(r))$. With r_* the unique minimizer established in Lemma 3.1 below, put $P_* = P(r_*)$ and $E_* = F(r_*)$. Numerically,

$$r_* \approx 0.7105483340929538, \qquad h_* \approx 0.7036483958041318, \qquad E_* \approx 25.75998653126983156.$$

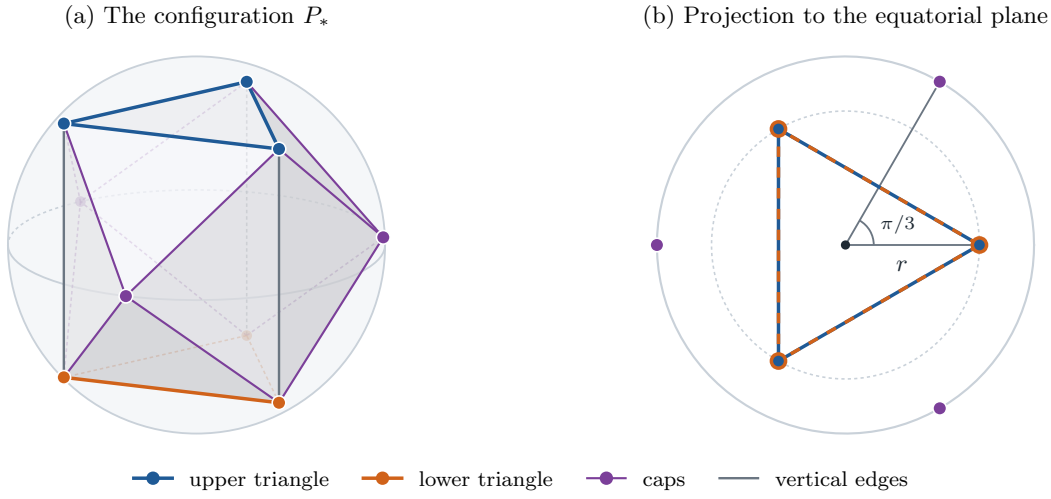


FIGURE 1. The tricapped trigonal prism. Two aligned triangles lie at opposite heights, and the three equatorial caps face the rectangular sides of the prism. (a) The configuration P_* inscribed in the sphere, with the edges of its convex hull; hidden edges are dashed. (b) Orthogonal projection to the equatorial plane. The two triangles project onto the same triangle, inscribed in the circle of radius r, and each cap is rotated by $\pi/3$ from the nearest triangle vertex.

The two triangles are aligned, occupying the same three longitudes, and each cap lies midway in longitude between two of them. Figure 1 shows the configuration at the optimal radius.

3.1.1. *Pairwise inner products.* By (2), the energy is determined by the pairwise inner products. Table 3 lists the six expressions for inner products in $P(r)$. For example, two triangle vertices on the same vertical line have inner product $r^2 - h^2 = 2r^2 - 1$. A cap differs in longitude by $\pi/3$ from four triangle vertices and by π from the remaining two, giving inner products $r/2$ and $-r$ respectively.

TABLE 3. The 36 pairs of the prism. At $r = r_*$ the six inner products form the target set $\mathcal{A}$. Labels are not in numerical order.

Label	Inner product	Pair type	Count
0	$-1/2$	Two caps	3
1	$1 - 3r^2/2$	Within one triangle	6
2	$2r^2 - 1$	Vertically aligned triangle vertices	3
3	$(r^2 - 2)/2$	Other pairs between the triangles	6
4	$r/2$	Cap and nearby triangle vertex	12
5	$-r$	Cap and distant triangle vertex	6

Summing the contributions gives

$$F(r) = \sqrt{3} + \frac{2\sqrt{3}}{r} + \frac{3}{2\sqrt{1-r^2}} + \frac{6}{\sqrt{4-r^2}} + \frac{12}{\sqrt{2-r}} + \frac{6}{\sqrt{2+2r}}. \tag{5}$$

Lemma 3.1. *The function F is strictly convex on $(0,1)$ and has exactly one critical point r_*, which is therefore its unique minimizer. The point r_* lies between two consecutive rationals with denominator 10^{80}, given in Appendix A, and $E_* < 644/25 = 25.76$.*

Proof. Every nonconstant summand in (5) is strictly convex. For the terms involving a quadratic expression this follows from

$$\frac{d^2}{dr^2}(c-r^2)^{-1/2} = \frac{c+2r^2}{(c-r^2)^{5/2}} > 0;$$

the remaining terms are positive multiples of $1/r$ or of negative powers of positive affine functions. Moreover $F'(r) \to -\infty$ as $r \downarrow 0$ and $F'(r) \to +\infty$ as $r \uparrow 1$, so strict convexity gives a unique zero of F'. Interval evaluation shows that F' is negative at the lower endpoint of the bracket and positive at the upper endpoint, and encloses F on the whole bracket. □

3.1.2. *Stationarity on the product of spheres.* The equation $F'(r_*) = 0$ expresses stationarity along the family. By symmetry, P_* is in fact stationary in every tangent direction, which is needed for the second-order argument of Section 9.

Lemma 3.2. *At P_* the ambient energy gradient at each point is radial:*

$$\nabla_i E = \lambda_i p_i, \qquad \lambda_i = -\frac{1}{2}\sum_{j\neq i}\|p_i - p_j\|^{-1}.$$

Consequently P_* is a critical point of E on $(\mathbb{S}^2)^9$.

Proof. A cap is fixed by the reflection in the equatorial plane and by the reflection in its own meridian plane. The first forces the vertical component of its tangential gradient to vanish and the second the azimuthal component. For a triangle vertex, the reflection in its meridian plane forces the azimuthal component to vanish, leaving the tangent direction in which the radius r changes. Rotations by $2\pi/3$ and the equatorial reflection permute the six triangle vertices together with these variations in r, so the six directional derivatives agree. Their sum is $F'(r_*) = 0$, hence each vanishes, and every gradient is radial. Finally,

$$\nabla_i E = -\sum_{j\neq i}\frac{p_i - p_j}{\|p_i - p_j\|^3}, \qquad p_i \cdot (p_i - p_j) = \frac{1}{2}\|p_i - p_j\|^2,$$

which gives the formula for λ_i. □

3.2. **The capped square antiprism.** For $0 < a < 1$, put $h = \sqrt{a}$ and $r = \sqrt{1-a}$, and let $P(a)$ consist of

$$\begin{aligned}
&(0,0,1),\ (0,0,-1),\\
&(r\cos(j\pi/2), r\sin(j\pi/2), h), \quad 0 \le j \le 3,\\
&(r\cos(\pi/4 + j\pi/2), r\sin(\pi/4 + j\pi/2), -h), \quad 0 \le j \le 3,
\end{aligned}$$

indexed in the order listed: $0, 1$ are the poles, $2, \dots, 5$ the upper square and $6, \dots, 9$ the lower square. Set $F(a) = E(P(a))$, let a_* be its unique minimizer (Lemma 3.3), and put $P_* = P(a_*)$, $E_* = F(a_*)$. Numerically,

$$a_* \approx 0.1786646584449405, \qquad h_* \approx 0.4226874240, \qquad E_* \approx 32.7169494601.$$

Figure 2 shows the configuration at $a = a_*$.

Table 4 lists the pairwise inner products and their multiplicities. The two poles contribute one pair with inner product -1. A pole has inner product h with the four ring points of the nearer square and $-h$ with the four others; counting both poles gives eight pairs of each kind. The pairs within one square and between the two squares give the remaining rows. Writing $c_\pm = -a \pm (1-a)/\sqrt{2}$, we obtain

$$F(a) = \phi(-1) + 8\phi(-\sqrt{a}) + 8\phi(\sqrt{a}) + 8\phi(a) + 4\phi(2a-1) + 8\phi(c_-) + 8\phi(c_+). \tag{6}$$

The target set $\mathcal{A}$ consists of the seven inner products at $a = a_*$. A fully expanded expression for F is given in Appendix B.

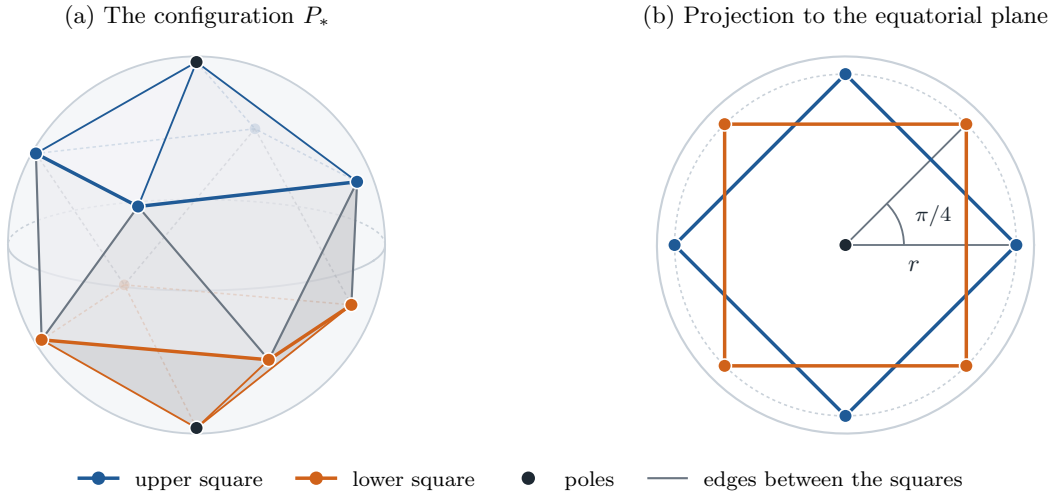


FIGURE 2. The capped square antiprism. The upper and lower squares differ in longitude by $\pi/4$, and two antipodal poles complete the configuration. (a) The configuration P_* inscribed in the sphere, with the edges of its convex hull; hidden edges are dashed. (b) Orthogonal projection to the equatorial plane. Both squares are inscribed in the circle of radius $r = \sqrt{1-a}$, and the two poles project to the center.

TABLE 4. The 45 pairs of the antiprism. At $a = a_*$ the seven inner products form the target set $\mathcal{A}$. Labels are not in numerical order.

Label	Inner product	Number of pairs
0	-1	1
1	$-\sqrt{a}$	8
2	$\sqrt{a}$	8
3	a	8
4	$2a-1$	4
5	$-a-(1-a)/\sqrt{2}$	8
6	$-a+(1-a)/\sqrt{2}$	8

3.2.1. *The optimal height.*

Lemma 3.3. *The function F is strictly convex on $(0,1)$ and has a unique minimizer a_* there. Its derivative has opposite strict signs at the two rational endpoints given in Appendix B.1.*

Proof. The power series of $(1-z)^{-1/2}+(1+z)^{-1/2}$ contains only even powers of z, with positive coefficients. Substituting $z=\sqrt{a}$ gives a power series in a with positive coefficients, including positive coefficients in every degree at least two, so this term of (27) is strictly convex. Each remaining nonconstant term of (27) is a positive multiple of a positive affine function raised to the power $-1/2$, and is strictly convex. The right derivative at 0 equals

$$5\sqrt{2}+1-\frac{4(2+\sqrt{2})}{(2-\sqrt{2})^{3/2}}-\frac{4(2-\sqrt{2})}{(2+\sqrt{2})^{3/2}}<0,$$

where the inequality is checked with rational interval arithmetic, and the derivative tends to $+\infty$ as $a\uparrow 1$. Strict convexity yields existence and uniqueness of the minimizer, and validated evaluations of F' at the two endpoints establish the stated bracket. □

3.2.2. *Stationarity on the full configuration space.*

Lemma 3.4. *The configuration P_* is a critical point of E on $(\mathbb{S}^2)^{10}$. Its ambient energy gradient satisfies*

$$\nabla_i E = \lambda_i p_i, \qquad \lambda_i = -\frac{1}{2}\sum_{j\neq i}\|p_i - p_j\|^{-1}.$$

Proof. A quarter turn about the polar axis fixes each pole and permutes the remaining points. Its fixed space is the polar axis, so the gradients at the poles have no tangential component. The reflection in the vertical plane through a ring point preserves the configuration and annihilates the azimuthal component of the gradient at that point. The remaining tangent line is spanned by the derivative of that point under a change of height. The quarter turns, together with the rotation by $\pi/4$ followed by the reflection in the equatorial plane, act transitively on the eight ring points and preserve this height variation. The eight directional derivatives therefore agree; their sum is $\frac{d}{dh}F(h^2) = 0$ at $h = h_*$, so each vanishes and every gradient is radial. The formula for λ_i follows exactly as in Lemma 3.2. □

4. Positive kernels and summation identities

Throughout, $N \in \{9, 10\}$, $C_N = \binom{N}{2}$ and $T_N = \binom{N}{3}$. For three unit vectors with pairwise inner products u, v, t, the Gram determinant is

$$\Delta(u,v,t) = \det\begin{pmatrix} 1 & u & v \\ u & 1 & t \\ v & t & 1 \end{pmatrix} = 1 + 2uvt - u^2 - v^2 - t^2 \geq 0;$$

it is the squared volume of the parallelepiped spanned by the three vectors. Every 4×4 Gram determinant of a configuration vanishes, since the vectors lie in $\mathbb{R}^3$. These two facts underlie the domain restrictions and the classification below.

4.1. **Two-point positivity.** Let L_k be the Legendre polynomial of degree k, normalized by $L_k(1) = 1$. The addition theorem for spherical harmonics gives

$$S_k(X) := \sum_{i,j=0}^{N-1} L_k(x_i \cdot x_j) \geq 0; \tag{7}$$

see Appendix E. For $k = 1$ this is $S_1 = \|\sum_i x_i\|^2$. If $g = \sum_{k=0}^{d} a_k L_k$ with $a_k \geq 0$ for $k \geq 1$, then

$$\sum_{i<j} g(t_{ij}) = B_N(g) + \frac{1}{2}\sum_{k\geq 1} a_k S_k(X) \geq B_N(g), \qquad B_N(g) = C_N a_0 - \frac{N}{2}\sum_{k\geq 1} a_k, \tag{8}$$

the correction $N/2$ accounting for the diagonal terms when passing from ordered to unordered pairs. Consequently, if $g \leq \phi$ on a set containing all pairwise inner products of X, then $E_N(X) \geq B_N(g)$; retaining the gap at one chosen pair gives the stronger inequality $E_N(X) \geq B_N(g) + \phi(t_{ij}) - g(t_{ij})$.

4.2. **Three-point positivity from planar projections.** Fix a unit vector x, choose orthonormal coordinates in $x^\perp$, and identify the orthogonal projection of a unit vector y onto $x^\perp$ with a complex number z_y. For $u = x \cdot y$, $v = x \cdot z$ and $t = y \cdot z$,

$$\mathrm{Re}(z_y\overline{z_z}) = t - uv, \qquad |z_y\overline{z_z}|^2 = (1-u^2)(1-v^2).$$

Define polynomials $Q_k \in \mathbb{Q}[u,v,t]$ by

$$Q_0 = 1, \quad Q_1 = t - uv, \quad Q_{k+2} = 2(t-uv)Q_{k+1} - (1-u^2)(1-v^2)Q_k. \tag{9}$$

The recurrence for the real parts of powers of a complex number gives $Q_k(u,v,t) = \mathrm{Re}(z_y^k \overline{z_z}^k)$. Hence, for every real polynomial p,

$$\sum_{y,z} p(x\cdot y)\, p(x\cdot z)\, Q_k(u,v,t) = \Big|\sum_{y} p(x\cdot y) z_y^k\Big|^2 \geq 0, \tag{10}$$

the sums running over the points of a configuration. For $k=0$ we set $z^0=1$, also when $z=0$; thus repeated indices and antipodal points are included and no division by a projection length occurs.

Positive semidefiniteness of the coefficient matrices below is established by explicit rational factorizations $B = CC^T$, which give $v^T B v = \|C^T v\|^2$. Equivalently, the factors specify the polynomials p in (10), so that positivity follows from explicit sums of squares.

4.3. **Corrections for repeated indices.** Let Sym denote averaging over the six permutations of (u,v,t). For a finite collection of real polynomials $p_{k\ell}$ put

$$A = \mathrm{Sym} \sum_{k,\ell} Q_k(u,v,t)\, p_{k\ell}(u)\, p_{k\ell}(v),$$

and let $\Psi_X A$ be the sum of A over all N^3 ordered triples of points of X, repetitions allowed. Summing (10) over the base point x shows $\Psi_X A \geq 0$; symmetrization does not change the full sum. Define

$$\mathcal{K}_{A,N} = (N-2)A(u,v,t) + A(u,u,1) + A(v,v,1) + A(t,t,1) + \frac{A(1,1,1)}{N-1}, \tag{11}$$

$$\mathcal{K}_{L,N} = \sum_{k\geq 1} c_k \left(\frac{L_k(u)+L_k(v)+L_k(t)}{3} + \frac{1}{N-1} \right), \qquad c_k \geq 0. \tag{12}$$

Lemma 4.1. *Summing over the unordered triples T of distinct points of X,*

$$\sum_T \mathcal{K}_{A,N}(T) = \frac{N-2}{6} \Psi_X A \geq 0, \qquad \sum_T \mathcal{K}_{L,N}(T) = \frac{N-2}{6} \sum_k c_k S_k(X) \geq 0.$$

Moreover, for every function f of one variable,

$$\sum_T \frac{f(u_T)+f(v_T)+f(t_T)}{3} = \frac{N-2}{3} \sum_{i<j} f(t_{ij}). \tag{13}$$

Proof. Each pair lies in $N-2$ triples, which proves (13). In the full ordered sum of A, the triples of distinct indices contribute $6\sum_T A(T)$, those with exactly two equal indices contribute $6\sum_{i<j} A(t_{ij}, t_{ij}, 1)$, and the diagonal contributes $NA(1,1,1)$. Summing (11) over T gives exactly $(N-2)/6$ times these contributions, because $T_N/(N-1) = N(N-2)/6$. Finally, $S_k = N + 2\sum_{i<j} L_k(t_{ij})$ gives the identity for $\mathcal{K}_{L,N}$. □

The factor $(N-2)/6$ equals $7/6$ for the prism and $4/3$ for the antiprism, and the factor in (13) equals $7/3$ and $8/3$ respectively. The kernels need not be pointwise nonnegative; their sums are nonnegative for every configuration.

5. Domain reduction: separation of competitive pairs

The first step adds a valid inequality to the problem: every competitive configuration satisfies $t_{ij} < b_N$ for all $i \neq j$. Since every minimizer is competitive, the later relaxations may be posed on the smaller domain. Precisely, we show that every triple of distinct points in a competitive configuration has its inner products in

$$D_{b_N} = [-1, b_N]^3 \cap \{\Delta \geq 0\}.$$

On this domain the factors $b_N - u$, $b_N - v$, $b_N - t$ are nonnegative and may serve as multipliers for polynomial squares, as in the sum-of-squares certificates of positivity on semialgebraic sets [19]. For the prism a two-point bound suffices; the antiprism also requires a three-point bound.

5.1. **Nine points.** Let X be competitive. The other 35 pairs each contribute at least $1/2$ to the energy, since no chord of the unit sphere is longer than 2. Hence, by Lemma 3.1, $\phi(t_{ij}) < \frac{644}{25} - \frac{35}{2} = \frac{413}{50}$, that is,

$$t_{ij} < 1 - \frac{1}{2(413/50)^2} = \frac{169319}{170569} < \frac{993}{1000} =: c. \tag{14}$$

Proposition 5.1. *There is a polynomial $g = \sum_{k=0}^{14} a_k L_k$ with rational coefficients, $a_k \geq 0$ for $k \geq 1$, such that*

$$B = 36a_0 - \frac{9}{2}\sum_{k\geq 1} a_k = \frac{12864300814989}{500000000000}$$

and

$$1 - (2-2t)g(t)^2 \geq 0, \qquad -1 \leq t \leq c,$$
$$1 - (2-2t)\big[g(t) + 644/25 - B\big]^2 \geq 0, \qquad b \leq t \leq c, \qquad b = 567/1000.$$

The coefficients of g are deposited in [29]. Both inequalities are polynomial inequalities with rational coefficients; they are proved by exact Bernstein expansion (Section 10.4) on a subdivision of the first interval into 23 subintervals and on the second interval as a whole.

Lemma 5.2. *Every competitive configuration has $t_{ij} < b = 567/1000$ for all $i \neq j$.*

Proof. The first inequality of Proposition 5.1 gives $g \leq \phi$ on $[-1, c]$, and the second gives $g + 644/25 - B \leq \phi$ on $[b, c]$. (Both conclusions hold even where the polynomials are negative, since the inequalities bound their absolute values by ϕ.) Suppose some pair had $t_{ij} \geq b$; by (14) it lies in $[b, c]$. Retaining its gap in (8) gives

$$E(X) \geq B + \phi(t_{ij}) - g(t_{ij}) \geq 644/25 > E_*,$$

contradicting competitiveness. □

Hence every triple of a competitive configuration lies in $D_b = [-1, b]^3 \cap \{\Delta \geq 0\}$. This domain includes its boundary $\Delta = 0$; for instance, the three caps of the candidate form such a degenerate triple.

5.2. **Ten points.** We prove that every competitive pair has inner product less than $b = 23/50$, that is, distance greater than $\sqrt{27/25}$. A fixed pair belongs to eight triples, one for each remaining point. If its inner product were too large, each of these triples would contribute a definite positive amount to a slack whose total is controlled by the energy.

Let X be competitive. Since $E_* < 33$ and the other 44 pairs contribute at least 22, every pair has energy less than 11, hence distance greater than $1/11$, and

$$t_{ij} < 241/242 < 249/250. \tag{15}$$

For $g = \sum_{j=0}^{d} a_j L_j$ with $a_j \geq 0$ for $j \geq 1$, (8) reads

$$E \geq B(g) = 45a_0 - 5\sum_{j\geq 1} a_j \tag{16}$$

whenever $g \leq \phi$ on the relevant interval, and retaining the gap at one pair gives $E \geq B(g) + \phi(t_{ij}) - g(t_{ij})$. We use two such polynomials in succession. Each satisfies $g \leq \phi$ on the current interval and

$$B(g) + \phi(t) - g(t) \geq \frac{654339}{20000} > E_*$$

on the tail to be excluded. The first excludes $[79/125, 249/250]$ from $[-1, 249/250]$, and the second excludes $[6273/10000, 79/125]$ from $[-1, 79/125]$.

Proposition 5.3. *There exist rational certificates with the following properties.*

(1) *Two scalar polynomials as above show successively that every competitive configuration satisfies* $t_{ij} < 79/125$ *and then* $t_{ij} < c = 6273/10000$.
(2) *There is a symmetric polynomial* $p = e/45 + \mathcal{K}_A + \mathcal{K}_L$ *with rational coefficients, where* $e = 3271693/100000$ *and the kernels have the form of Section 4, such that*

$$\sigma(u,v,t) = \frac{\phi(u)+\phi(v)+\phi(t)}{3} - p(u,v,t) \geq 0 \quad \text{on } [-1,c]^3 \cap \{\Delta \geq 0\}.$$

(3) *On the closed subdomain* $u, v \in [-1, c]$, $t \in [23/50, c]$, $\Delta \geq 0$, *the same function satisfies* $\sigma \geq \beta = 1/150000$.

The certificates are deposited in [30]. Item 1 is proved by exact Bernstein expansion, and items 2 and 3 by Bernstein bounds on boxes in validated arithmetic (Section 10.4). The same polynomial p is used in items 2 and 3.

Lemma 5.4. *Every competitive configuration has* $t_{ij} < b = 23/50$ *for all* $i \neq j$.

Proof. By Lemma 4.1 and item 2 of Proposition 5.3,

$$0 \leq \sum_T \sigma(T) \leq \frac{8}{3}(E - e).$$

If some pair had inner product at least b, the eight triples containing it would each contribute at least β by item 3, and the remaining 112 triples would contribute nonnegatively. Hence

$$E \geq e + 3\beta = \frac{654339}{20000} = 32.71695 > E_*,$$

a contradiction; the final strict inequality holds uniformly on the parameter bracket of Lemma 3.3. □

The argument uses eight triples of one actual configuration; it does not assume that arbitrarily chosen admissible triples can be realized simultaneously. The endpoints $t = b$ and the boundary $\Delta = 0$ are included in the verified domains. Consequently every triple of a competitive configuration lies in D_b.

6. A near-tight rational lower bound

This section constructs the dual certificate: a rational three-point identity which, summed over a configuration, bounds the energy from below. Its residual is not zero but is bounded explicitly, and the resulting bound is within 10^{-50} of the optimal value (Corollary 6.4). The two certificates have the same structure, but the interpolation conditions differ because only the antiprism has an antipodal pair. Write $\epsilon_N = N - 9$, so that $\epsilon_9 = 0$ and $\epsilon_{10} = 1$, and put

$$\mathcal{B}_9 = \mathcal{A}_9, \qquad \mathcal{B}_{10} = \mathcal{A}_{10} \setminus \{-1\}.$$

Each $\mathcal{B}_N$ has six elements.

6.1. **Hermite minorants.** Let H_N be the polynomial of degree at most $11 + \epsilon_N$ that agrees with ϕ to first order at each node of $\mathcal{B}_N$ and, when $N = 10$, also agrees with ϕ at -1. Let $\widehat{H}_N$ be the polynomial of degree at most $15 + \epsilon_N$ with the same double contacts at $\mathcal{B}_N$ and a contact of order $4 + \epsilon_N$ at -1. Since the nodes are distinct, these Hermite interpolation problems have unique solutions.

Lemma 6.1. *Both* H_N *and* $\widehat{H}_N$ *lie below* ϕ *on* $[-1, 1)$. *The contact set of* H_N *with* ϕ *is exactly* $\mathcal{A}_N$, *and that of* $\widehat{H}_N$ *is* $\mathcal{A}_N \cup \{-1\}$.

Proof. For $n \geq 1$,

$$\phi^{(n)}(t) = 1 \cdot 3 \cdots (2n-1)\,(2-2t)^{-n-1/2} > 0.$$

Hermite's remainder formula gives, away from the nodes,

$$\phi(t) - H_N(t) = \frac{\phi^{(12+\epsilon_N)}(\xi)}{(12+\epsilon_N)!}(t+1)^{\epsilon_N} \prod_{\alpha \in \mathcal{B}_N} (t-\alpha)^2,$$

$$\phi(t) - \widehat{H}_N(t) = \frac{\phi^{(16+\epsilon_N)}(\zeta)}{(16+\epsilon_N)!}(t+1)^{4+\epsilon_N} \prod_{\alpha \in \mathcal{B}_N} (t-\alpha)^2, \tag{17}$$

with $\xi, \zeta \in (-1,1)$ depending on t. All factors are nonnegative on $[-1,1)$, and the products vanish only at the stated contacts. For completeness: if H has degree at most $n-1$ and w is the monic product of its n interpolation factors, put $\kappa = (\phi(t) - H(t))/w(t)$; the function $\phi(s) - H(s) - \kappa w(s)$ has $n+1$ zeros counted with multiplicity, and repeated application of Rolle's theorem yields $\phi^{(n)}(\xi) = \kappa\, n!$. □

6.2. **The rational identities.** Put $M_N = (H_N + \widehat{H}_N)/2$. The coefficients of M_N depend on the irrational parameter r_* or a_*; the certificate uses a rational polynomial m_N that approximates M_N from below. In the appendices, m, U, R, ρ without subscripts denote the quantities for the case at hand.

Proposition 6.2. *For each $N \in \{9, 10\}$ there are a rational polynomial m_N of degree $15 + \epsilon_N$, a rational number $U_N > E_N^*$, kernels $\mathcal{K}_{A,N}$ and $\mathcal{K}_{L,N}$ of the form (11)–(12) with rational coefficients, a polynomial $W_N \in \mathbb{Q}[u,v,t]$ and a polynomial $R_N \in \mathbb{Q}[u,v,t]$ such that*

$$\frac{m_N(u) + m_N(v) + m_N(t)}{3} - \frac{U_N}{C_N} = \mathcal{K}_{A,N} + \mathcal{K}_{L,N} + W_N + R_N \tag{18}$$

holds identically, $m_N \leq M_N$ on $[-1,1]$, $W_N \geq 0$ on D_{b_N}, and the residual satisfies

$$\rho_N := \sum_{\nu} |[u^{\nu_1} v^{\nu_2} t^{\nu_3}] R_N|, \qquad 72\rho_9 < 10^{-50}, \qquad 90\rho_{10} < 7.21 \times 10^{-57}. \tag{19}$$

Numerically,

$$\rho_9 \approx 1.90069467431976 \times 10^{-53}, \qquad \rho_{10} \approx 8.009784771683718 \times 10^{-59}.$$

Each residual has total degree 20 and 1041 nonzero coefficients. Since every monomial has modulus at most one on $D_{b_N} \subset [-1,1]^3$, we have $|R_N| \leq \rho_N$ on D_{b_N}. The residual has no prescribed sign; only its coefficient norm enters the argument.

The polynomial W_N is a sum of squares multiplied by the weights

$$1, \quad 1+u, \quad b_N - u, \quad \Delta, \quad (1+u)(b_N-u), \quad \Delta(1+u)(b_N-u),$$

each averaged over the permutations of (u,v,t); all these weights are nonnegative on D_{b_N}. There are 360 weighted squares for the prism and 336 for the antiprism. The kernels are nonnegative only after summation over a configuration, whereas W_N is nonnegative at every admissible triple. The Legendre part $\mathcal{K}_{L,N}$ uses L_1 for the prism and L_1, L_3 for the antiprism. Appendices A.1 and B.2 give U_N, the sizes of the factors and the bounds establishing $m_N \leq M_N$. The identity (18) is verified coefficient by coefficient in exact rational arithmetic.

Lemma 6.3 (Total interpolation gap)**.** *Every competitive configuration satisfies*

$$0 \leq \sum_{i<j} (\phi - H_N)(t_{ij}) < 2C_N \rho_N. \tag{20}$$

Proof. By Section 5, every triple of the configuration lies in D_{b_N}. Summing (18) over all triples and applying Lemma 4.1 gives

$$\frac{N-2}{3}\Big(\sum_{i<j} m_N(t_{ij}) - U_N\Big) \geq -T_N\rho_N.$$

Since $3T_N/(N-2) = C_N$, it follows that $\sum_{i<j} m_N(t_{ij}) \geq U_N - C_N\rho_N$. As $E_N(X) \leq E_N^* < U_N$, we get $\sum_{i<j}(\phi - m_N)(t_{ij}) < C_N\rho_N$. Finally, by Lemma 6.1,

$$\phi - m_N \geq \phi - M_N = \tfrac{1}{2}[(\phi - H_N) + (\phi - \widehat{H}_N)] \geq \tfrac{1}{2}(\phi - H_N) \geq 0,$$

which gives (20), with $2C_9 = 72$ and $2C_{10} = 90$. □

Corollary 6.4 (Near-tight global lower bound)**.** *For $N \in \{9, 10\}$, every configuration X of N distinct points on $\mathbb{S}^2$ satisfies*

$$E_N(X) > E_N^* - C_N\rho_N.$$

In particular $E_9(X) > E_9^* - 10^{-51}$ and $E_{10}(X) > E_{10}^* - 10^{-56}$.

Proof. If X is not competitive, then $E_N(X) > E_N^*$. Otherwise the proof of Lemma 6.3 gives $\sum_{i<j} m_N(t_{ij}) \geq U_N - C_N\rho_N$. Since $m_N \leq M_N \leq \phi$ on $[-1, 1)$ by Proposition 6.2 and Lemma 6.1, we obtain $E_N(X) \geq \sum_{i<j} m_N(t_{ij}) \geq U_N - C_N\rho_N > E_N^* - C_N\rho_N$. The numerical bounds follow from $36\rho_9 < 10^{-51}$ and $45\rho_{10} < 10^{-56}$. □

Remark 6.5 (Interpretation as a dual certificate). The kernels $\mathcal{K}_{A,N}$ and $\mathcal{K}_{L,N}$ are built from positive semidefinite matrices and W_N is a weighted sum of squares, so the identity (18) is a feasible solution, with rational data, of the dual of a three-point semidefinite relaxation of problem (1) restricted to D_{b_N}. Corollary 6.4 says that its duality gap is less than $C_N\rho_N$. If the gap were zero, complementary slackness would force every pair inner product of a minimizer into the contact set of M_N with ϕ, which is $\mathcal{A}_N$ by Lemma 6.1. Lemma 6.3 is the quantitative substitute: a competitive configuration has total slack less than $2C_N\rho_N$ in the inequality $\phi \geq H_N$. Section 7 converts this small slack into proximity to $\mathcal{A}_N$.

7. Quantitative complementary slackness: localization of pair values

A small interpolation gap forces the argument to be close to a contact node. This is the mechanism by which the near-zero duality gap of Corollary 6.4 constrains the competitors. For example, $f(t) = 1 + t^4$ and $H(t) = 15/16 + t^2/2$ satisfy $f(t) - H(t) = (t^2 - 1/4)^2$. If $d(t)$ denotes the distance from t to the nearer of $\pm 1/2$, the distance to the other node is at least $1/2$, so $f - H \geq d(t)^2/4$; see Figure 3.

Lemma 7.1 (Quantitative Hermite gap)**.** *For $N \in \{9, 10\}$ and $-1 \leq t \leq b_N$,*

$$\phi(t) - H_N(t) \geq 10^{-12}\,\mathrm{dist}(t, \mathcal{A}_N)^2. \tag{21}$$

Proof. The derivative of ϕ appearing in (17) is positive and increasing on $[-1, 1)$, so it is bounded below by its value at -1. For the prism this gives

$$\phi(t) - H_9(t) \geq \gamma_9 \prod_{\alpha \in \mathcal{A}_9} (t - \alpha)^2, \qquad \gamma_9 = \frac{\binom{24}{12}}{2^{37}}.$$

Partition $[-1, b_9]$ at the midpoints between consecutive nodes. On each cell, divide by the square of the distance to the node in that cell, and bound each remaining factor from below by its value at the nearer endpoint of the cell. Using rational enclosures of the nodes, this gives six explicit lower bounds, the smallest of which, multiplied by γ_9, exceeds 1.874×10^{-11}.

For the antiprism, the nodes in increasing order are

$$-1, \quad c_-, \quad 2a_* - 1, \quad -h_*, \quad a_*, \quad c_+, \quad h_*,$$

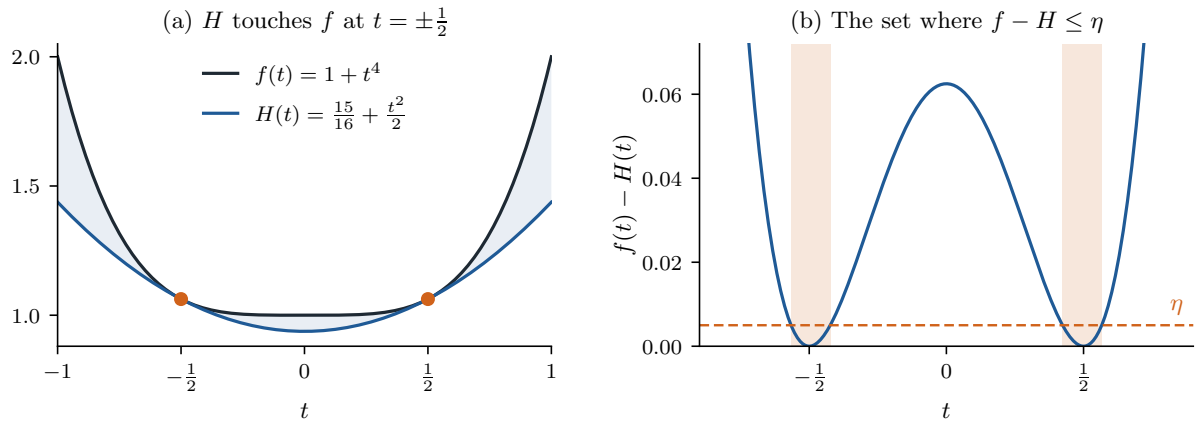


FIGURE 3. Localization by a nonnegative interpolation gap. Left: f and H touch at $\pm 1/2$. Right: the shaded intervals are where $f - H \le \eta$, with $\eta = 0.005$. The Coulomb estimates rest on the same principle, with six or seven contacts.

and the remainder formula gives

$$\phi(t) - H_{10}(t) \ge \gamma_{10}(t+1) \prod_{\alpha \in \mathcal{B}_{10}} (t-\alpha)^2, \qquad \gamma_{10} = \frac{\binom{26}{13}}{2^{40}}.$$

We use seven midpoint cells covering $[-1, 7841/12500] \supset [-1, b_{10}]$. On every cell except the one containing -1, we divide by the squared distance to its node, bound the remaining squared factors as above, and bound $t+1$ from below at the left endpoint. On the cell containing -1 we have $0 \le t+1 \le 1$, hence $t+1 \ge (t+1)^2$, and we divide by $(t+1)^2$. The smallest of the resulting products, multiplied by γ_{10}, exceeds 7.87×10^{-12}.

These finitely many products are bounded below using outward-rounded interval arithmetic over the full parameter brackets. Both bounds exceed 10^{-12}. At a node both sides of (21) vanish. □

Corollary 7.2. *Every competitive configuration satisfies* $\operatorname{dist}(t_{ij}, \mathcal{A}_N) < \delta_N$ *for all* $i \ne j$, *where* $\delta_9 = 10^{-19}$ *and* $\delta_{10} = 10^{-22}$.

Proof. Each summand in (20) is nonnegative. For $N = 9$, Lemma 7.1 gives $10^{-12} \operatorname{dist}(t_{ij}, \mathcal{A}_9)^2 < 72\rho_9 < 10^{-50} = 10^{-12}\delta_9^2$. For $N = 10$ the corresponding bound is $90\rho_{10} < 7.21 \times 10^{-57} < 10^{-56} = 10^{-12}\delta_{10}^2$. □

The parameter brackets show that distinct targets differ by more than $1/100$ for the prism and by more than $1/50$ for the antiprism, so each pair has a unique nearby target. It remains to show that these targets fit together under a single labeling of the points.

8. Recovery of a common labeling

Corollary 7.2 does not say which target belongs to which pair. We recover a common labeling from the rank condition on the Gram matrix. This is the nonconvex constraint that the positivity relaxations of Sections 4–6 do not use; reimposing it here identifies the primal solution from the approximate pair values. For the finite exclusions we use the larger radii $\eta_9 = 10^{-9}$ and $\eta_{10} = 10^{-5}$, which dominate the actual errors δ_N.

8.1. **Three anchors determine the remaining products.** Let a_1, a_2, a_3 be linearly independent unit vectors, let C be the matrix with these columns, and put $A = C^T C$ and $b_x = C^T x$. Solving for x in the basis a_1, a_2, a_3 gives

$$x \cdot y = b_x^T A^{-1} b_y. \tag{22}$$

Thus once the inner products of x and y with the anchors are known, the inner product $x \cdot y$ is determined; see Figure 4. In polynomial form,

$$\det \begin{pmatrix} A & b_y \\ b_x^T & t \end{pmatrix} = 0, \qquad t = x \cdot y, \tag{23}$$

since the determinant equals $\det(A)\,(t - b_x^T A^{-1} b_y)$. Taking $y = x$ and $t = 1$ gives the condition that a proposed vector b_x comes from a unit vector.

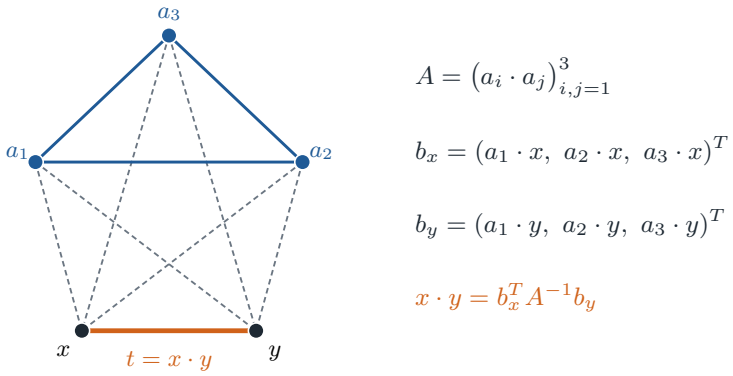


FIGURE 4. Three common anchors constrain every pair of further points. The dashed edges give the inner products of x and y with the anchors; the inner product of x and y (orange edge) is then determined by (22).

8.2. **Existence of a well-conditioned anchor triple.** Let $M_X = \sum_i x_i x_i^T$, so that $\operatorname{tr} M_X = N$ and

$$S_2(X) = \frac{3}{2}\Big(\operatorname{tr}(M_X^2) - \frac{N^2}{3}\Big)$$

(Appendix E). If the least eigenvalue of M_X is $N/3 - d$, the deviations of the other two eigenvalues from $N/3$ sum to d, so the squared deviations of all three sum to at least $d^2 + d^2/2$; hence $S_2 \geq 9d^2/4$.

For the prism let g_9 be the polynomial of Proposition 5.1, and for the antiprism let g_{10} be the first scalar polynomial of Proposition 5.3. Their coefficients of L_2 are

$$a_{2,9} = \frac{1024990614517}{5000000000000}, \qquad a_{2,10} = \frac{16963462314052}{65569774397283}.$$

Retaining the S_2 term in (8) gives

$$S_2(X) \leq \frac{2(E_N(X) - B_N(g_N))}{a_{2,N}}.$$

Using $E_9^* < 644/25$ and $E_{10}^* < 32717/1000$ we obtain:

	Prism	Antiprism
$S_2(X)$	$< 9/25$	$< 1/3$
$\lambda_{\min}(M_X)$	$> 13/5$	$> 29/10$

(The polynomials g_N minorize ϕ on the initial domains of Section 5.) By the Cauchy–Binet formula,

$$\sum_{|I|=3} \det G_I = \det M_X,$$

where G_I is the Gram matrix of the triple I. There are 84 triples for the prism and 120 for the antiprism, and

$$\frac{(13/5)^3}{84} > \frac{1}{5}, \qquad \frac{(29/10)^3}{120} > \frac{1}{5}.$$

Hence some triple of points of X has Gram determinant greater than $1/5$. In particular, no competitive configuration lies in a plane through the origin.

8.3. **Perturbation bounds for determinants.** Replace each inner product by its nearby target. Along the segment from the actual entries to the targets every entry stays in $[-1, 1]$, so telescoping the products in the Leibniz expansion gives the following bounds:

Determinant	Perturbation bound
3×3 Gram matrix with unit diagonal	$12\eta_N$
4×4 Gram matrix with unit diagonal	$72\eta_N$
4×4 mixed minor (23)	$78\eta_N$

There are respectively 6, 12 and 13 variable matrix entries, counting the two occurrences of each symmetric off-diagonal entry separately. Each entry changes by at most η_N, and its cofactor has modulus at most $2! = 2$ or $3! = 6$, since all entries stay in $[-1, 1]$. Integrating the determinant derivative along the segment gives the constants $6 \cdot 2$, $12 \cdot 6$ and $13 \cdot 6$. Every 4×4 minor of the actual Gram matrix, including (23), vanishes because the Gram matrix has rank at most three.

For the antiprism, when the bound $72\eta_{10}$ is inconclusive, we use instead

$$|\det G - \det G_{\text{target}}| \le \eta_{10} \sum_{l=1}^{6} \sup_{\text{box}} |\partial_l \det|,$$

where the supremum is taken over the box of radius η_{10} about the target entries, intersected with $[-1, 1]$ in each coordinate, which contains the segment to the actual Gram matrix. This refinement is used only to justify exclusions.

8.4. **Exhaustive classification.** The following procedure is applied separately to the two target sets.

(1) Enumerate unordered triples of target labels for the anchor triangle, and retain those whose determinant, increased by $12\eta_N$, exceeds $1/5$. Restricting to sorted triples loses nothing, since every permutation of the three edges of a triangle is induced by a permutation of its vertices.
(2) For each retained anchor triangle, enumerate all possible vectors of target labels from a further point to the anchors: $6^3 = 216$ for the prism and $7^3 = 343$ for the antiprism. Discard such a *description* only if its unit-length determinant is provably incompatible with rank three.
(3) For every pair of retained descriptions and every possible label of the mutual inner product, apply the mixed-minor test (23). Equal descriptions are tested as well: it is not assumed that distinct points have distinct descriptions.
(4) Form the graph whose vertices are the retained descriptions, joined by an edge labeled with each retained mutual label. Enumerate all $(N-3)$-cliques, adjoin the anchors, and compare the resulting labeled Gram matrix with that of the candidate. Here an isomorphism is a relabeling of the points preserving all target labels.

Every actual configuration gives rise to a retained clique. The converse need not hold: the graph is an outer approximation, which suffices for an argument by exclusion.

Proposition 8.1. *With the radii η_N, the procedure produces the counts in Table 5. All duplicate descriptions are excluded. Every surviving clique carries a unique target label on each edge and, after adjoining its anchors, is isomorphic to the labeled Gram matrix of the candidate.*

TABLE 5. The exhaustive classifications for the two target sets. In the antiprism graph, three retained descriptions with nonvanishing norm polynomial are isolated and lie in no seven-clique.

Test	Prism	Antiprism
Retained sorted anchor types	33	35
Unit-length tests on descriptions	7128	12005
Description tests requiring the derivative bound	0	83
Mixed mutual-label tests	540	1162
Duplicate-description tests	216	476
Surviving cliques	6 six-cliques	7 seven-cliques

For the prism, all quantities are computed as exact rational polynomials in r and enclosed by outward-rounded dyadic intervals over the parameter bracket. For the antiprism they are integer polynomials in h and $\sqrt{2}$, reduced by $(\sqrt{2})^2 = 2$, enclosed on the lattice $2^{-384}\mathbb{Z}$. In both cases determinants are expanded by the Leibniz formula and the candidate Gram matrix is computed directly from coordinates. A polynomial identity is accepted only if all its coefficients vanish; a nonzero polynomial justifies an exclusion only when its enclosure is separated from zero.

Corollary 8.2. *After relabeling, every competitive configuration satisfies*

$$|x_i \cdot x_j - p_i \cdot p_j| < \delta_N \qquad (i \neq j), \qquad P_N^* = (p_0, \dots, p_{N-1}).$$

Proof. The well-conditioned anchor triple passes the first test. The remaining points give retained descriptions, which are pairwise distinct by the duplicate tests and form a surviving clique. The isomorphism of Proposition 8.1 provides a common labeling. Since the labels are now fixed, the actual errors are those of Corollary 7.2, namely less than δ_N; the larger radius η_N was only used for exclusions. □

9. ALIGNMENT AND STRICT LOCAL MINIMALITY

The labeled Gram matrix determines the configuration up to an orthogonal transformation. A quantitative alignment places the points in the charts used for the local Hessian bound. Because the objective is invariant under $O(3)$, the Hessian at the candidate is singular in the directions of the group orbit; the second-order condition is therefore imposed on a slice transversal to the orbit. A positive definite Hessian at the candidate alone would give strict local minimality on some unspecified neighborhood. To connect with the global localization, we certify a uniform Hessian bound on an explicit box whose radius exceeds the localization error.

9.1. **Coordinates modulo rotations.** At each candidate point p_i choose a 3×2 matrix B_i whose columns form an orthonormal basis of the tangent plane, and define

$$x_i(q_i) = \frac{p_i + B_i q_i}{\sqrt{1 + \|q_i\|^2}}, \qquad q_i = \frac{B_i^T x_i}{p_i \cdot x_i}; \tag{24}$$

the inverse is valid when $p_i \cdot x_i > 0$, and $q_i = 0$ corresponds to p_i. This gives $2N$ real coordinates. To remove the rotational freedom, we fix both coordinates of point 0 and one coordinate of a second point, which removes the rotations about p_0:

	Prism	Antiprism
Point 0	first vertex of the upper triangle	north pole
Second point	second vertex of the upper triangle	first vertex of the upper square
Coordinate fixed there	along $p_0 \times p_1$	azimuthal
Free coordinates	15	17

These conditions choose a slice for the action of $SO(3)$; they impose no restriction on the shape of a competitor. The frames are specified in Appendix D.

Lemma 9.1 (Quantitative alignment)**.** *If all labeled Gram errors are less than d, where $0 < d \le 10^{-9}$, then some element of $O(3)$ carries the configuration into the charts (24) with the three fixed coordinates equal to zero and every free coordinate of modulus less than $128d$.*

Sketch of proof. A polar decomposition aligns the actual and candidate anchor triples to within $2d$. Solving for each point from its three anchor inner products gives point errors less than $8d$. A minimal rotation fixing point 0 increases the errors to less than $16d$. A rotation about p_0 then moves the second point into its candidate meridian half-plane; since the candidate's distance from the axis exceeds $4/5$, this rotation is within $40d$ of the identity in operator norm, and all point errors become less than $56d$. The inverse chart has denominator greater than $1/2$, giving $\|q_i\| < 112d < 128d$. The details are in Appendix C. □

Proposition 9.2 (Validated local convexity)**.** *In the coordinates above, uniformly over the parameter brackets, the Hessian satisfies*

$$D^2E_N(q) \succeq I/1000 \quad \text{for } \|q\|_\infty \le s_N, \qquad s_9 = 10^{-7}, \quad s_{10} = 10^{-6}.$$

Consequently, at the exact optimal parameter,

$$E_N(q) \ge E_N^* + \|q\|^2/2000 \qquad (\|q\|_\infty \le s_N). \tag{25}$$

Proof. The Hessian bound on the whole box is established by validated computation, as described in Appendix D. By Lemmas 3.2 and 3.4, $q = 0$ is a critical point. For fixed q in the box set $f(t) = E_N(tq)$ for $0 \le t \le 1$. The segment stays in the box, $f'(0) = 0$ and $f''(t) = q^T D^2E_N(tq)q \ge \|q\|^2/1000$, hence

$$E_N(q) - E_N(0) = \int_0^1 (1-t)f''(t)\,dt \ge \|q\|^2/2000.$$ □

9.2. **Proof of the main theorem.**

Proof of Theorem 1.1. It suffices to consider configurations with $E_N(X) \le E_N^*$. By Lemmas 5.2 and 5.4, every triple of X lies in D_{b_N}. Lemma 6.3 and Corollary 7.2 place every inner product within δ_N of $\mathcal{A}_N$, and Corollary 8.2 provides a labeling under which all Gram errors are less than δ_N. By Lemma 9.1, after an orthogonal transformation,

$$\|q\|_\infty < 128\delta_N < s_N,$$

so (25) applies and, together with $E_N(X) \le E_N^*$, forces $q = 0$. Thus every competitive configuration is congruent to P_N^*. Conversely, congruent configurations have equal energy. □

No step assumes symmetry of the competitor, and neither antipodal pairs nor degenerate triples with $\Delta = 0$ are excluded. Configurations with coincident points have infinite energy and are not competitive.

10. Verification algorithms, certificate sizes and costs

The proof reduces statements about all configurations to three kinds of finite assertions: polynomial identities over $\mathbb{Q}$, an exhaustive finite classification, and inequalities on compact sets established by validated numerics. The analytic reductions (the kernel summation, the interpolation remainder, stationarity, the determinant perturbation bounds, alignment and the Taylor argument) are given in the main text and appendices. This section describes the algorithms that check the finite assertions. It treats two independent implementations: the archived checkers in exact and interval arithmetic [29, 30], and the Lean formalization. No inequality is accepted on the basis of an inconclusive bound. In the classification, an inconclusive exclusion test retains the case for further analysis.

10.1. **Certificate data.** Table 6 summarizes the certificates. The three-point certificate dominates. Its kernel blocks are given by rational factor columns in the Legendre basis, its weighted squares by rational columns in a tensor Chebyshev basis, and its residual by rational coefficients in the monomial basis. The detailed block dimensions are in Appendices A.1 and B.2.

TABLE 6. Sizes of the certificates. File sizes are those of the archived JSON files [29, 30].

	Prism	Antiprism
Three-point certificate file	10.2 MB	9.5 MB
Degree of the rational minorant m_N	15	16
Total degree of kernels and residual	20	20
Circle-kernel levels	10	10
Weighted squares, before symmetrization	360	336
Nonzero coefficients of the residual R_N	1041	1041
Residual norm ρ_N	1.90×10^{-53}	8.01×10^{-59}
Three-point separation certificate file	—	0.71 MB
Labeling certificate file	17.6 kB	35.7 kB

10.2. **Exact identities.** The identity (18) is verified coefficient by coefficient in $\mathbb{Q}[u, v, t]$, after expanding the potential term, the kernels, the weighted squares and the full signed residual. The Legendre polynomials are generated by Rodrigues' formula, and the circle kernels by the closed expression

$$Q_k = \sum_{j=0}^{\lfloor k/2 \rfloor} (-1)^j \binom{k}{2j} (t - uv)^{k-2j} \Delta^j,$$

which is the real part of $(t - uv + i\sqrt{\Delta})^k$ for $\Delta \geq 0$ and agrees with (9) as a polynomial identity. The certificates were found by numerical optimization, but no floating-point quantity enters their verification: all denominators and all Legendre coefficients are checked exactly. Positive semidefiniteness of each block needs no eigenvalue computation, because every block is given in the factored form CC^T.

10.3. **Interval arithmetic.** Real quantities are enclosed in intervals with outward rounding. A positive lower endpoint proves positivity; an interval containing zero proves neither a sign nor an identity. All parameter-dependent quantities are enclosed over the full rational bracket for r_* or a_*. The Hermite interpolation systems are preconditioned by a fixed approximate inverse and solved in 600-bit interval arithmetic; for the prism, a row-sum bound less than $1/2$ for the residual of the preconditioner proves its invertibility. The resulting coefficient enclosures justify the downward shifts 10^{-55} and 10^{-59} in the definition of m_N and the inequalities $U_N > E_N^*$, uniformly over the brackets.

10.4. **Bernstein bounds.** For a polynomial on an interval, the Bernstein basis is nonnegative and sums to one, so the smallest Bernstein coefficient is a lower bound [8]. The scalar inequalities in Propositions 5.1 and 5.3 are proved by exact conversion of rational polynomials to Bernstein form on rational subintervals whose union is the required interval.

The three-point inequalities of Proposition 5.3 involve the non-polynomial function ϕ. On each box, the positive Taylor coefficients of ϕ at the left endpoint give a polynomial lower bound for ϕ, and tensor-product Bernstein coefficients of the resulting polynomial slack are computed in binary64 interval arithmetic with outward rounding and propagated by de Casteljau subdivision. A box is accepted if its coefficients prove the required inequality, if the Gram determinant has a negative upper bound on it, or if for some $q \geq 0$ all Bernstein coefficients of the slack minus $q\Delta$ are

nonnegative (the choice of q is heuristic, but the resulting inequality is verified rigorously). On the symmetric global domain one may assume $u \le v \le t$; on the subdomain of item 3 only $u \le v$, since the range of t differs. The endpoints and the boundary $\Delta = 0$ are included, and a box is never accepted on account of its size alone.

10.5. **Classification and local Hessian.** The classification of Section 8 is computed from exact determinant polynomials, as described there; Table 5 gives the number of tests of each kind. Its cost is governed by the number of anchor types and descriptions, 6^3 or 7^3 per anchor, not by the size of the configuration space. The Hessian bounds of Proposition 9.2 are established on the entire boxes using Arb ball arithmetic [12], and independently with a separate implementation of integer interval arithmetic; both use the derivative formulas of Appendix D.

Apart from the mathematics of this paper, the correctness of the archived checkers thus rests on exact integer and rational arithmetic, on the FLINT and Arb libraries, on our interval implementations, and, for the three-point separation for $N = 10$, on IEEE 754 binary64 arithmetic with round-to-nearest and without contraction of floating-point operations. Numerical approximations of the parameters and the figures are not used in the proof. The formalization described next removes these dependencies.

10.6. **Formal verification in Lean.** Both theorems have been formalized in Lean 4 with Mathlib [6, 22]. For each N the formal statement asserts that the family parameter lies in the rational bracket of Appendix A or B.1, that it is the unique critical point of the family energy on $(0, 1)$, that every configuration of N distinct unit vectors has energy at least that of the candidate, and that equality holds exactly for the configurations obtained from the candidate by an orthogonal transformation and a relabeling. Both formal proofs are complete and depend only on the three standard axioms `propext`, `Classical.choice` and `Quot.sound`. In particular, no result of compiled code is accepted without kernel verification: all finite checks are run by kernel reduction (`decide +kernel`), not by `native_decide`.

The analytic reductions are proved in Lean. The certificate data are translated into Lean by generator scripts and checked by the Lean kernel, so the translation need not be trusted. Interval bounds are evaluated with exact rational arithmetic using operations whose correctness is proved in Lean. No floating-point computation is trusted; the certificate checks rely on the Lean kernel and its arbitrary-precision integer arithmetic.

10.6.1. *Making certificate-sized checks feasible in the kernel.* The kernel is fast on large integers, which it handles with GMP, and slow on recursion. In our measurements a list-recursion step costs about 0.3 ms regardless of the size of the numbers involved, and typeclass-generic operations are several times slower than specialized ones. Expanding certificate-sized trivariate polynomials as nested lists is therefore out of reach: a single square of a 165-term polynomial took about 40 s. Three techniques move the work from recursion into integer arithmetic.

Integer scaling and explicit formulas. Checks are stated over $\mathbb{Z}$ after clearing denominators, with explicit formulas instead of generic rational matrices. For the labeling classification this reduced the time from about 2.5 min per anchor triple over $\mathbb{Q}$ to about 75 s for all anchor triples over $\mathbb{Z}$.

A Kronecker zero test. Large identities, including the three-point identities (18), are checked by Kronecker substitution [26, 11]. The following elementary lemma, proved in Lean, makes the test sound.

Lemma 10.1 (Kronecker zero test)**.** *Let $p = \sum c_{abc} u^a v^b t^c \in \mathbb{Z}[u, v, t]$, and let $B \ge 1$ and $K \ge 2$ be integers such that $\deg_t p < B$ and $|c_{abc}| < K$ for all coefficients. If $p(u, K^B, K) = 0$ in $\mathbb{Z}[u]$, then $p = 0$.*

Proof. Fix a. The coefficient of u^a in $p(u, K^B, K)$ is $\sum_{b,c} c_{abc} K^{Bb+c}$, and since $c < B$ the exponents $Bb + c$ are distinct. If not all c_{abc} vanish, let e be the smallest exponent with a nonzero coefficient d_e. Then $d_e K^e \equiv 0 \pmod{K^{e+1}}$, so K divides d_e, which contradicts $0 < |d_e| < K$. □

The coefficients of p are never computed. They are bounded a priori by ℓ^1-norms of the factors, using $\|fg\|_1 \le \|f\|_1\|g\|_1$, and the degrees are bounded by degree boxes. All certificate columns are converted to the power basis with integer scalings, and the weighted square blocks $S_b = \sum_c P_c^2$ are checked separately in the same way. For the prism, the substitution is $v = K^{24}$, $t = K$ with $K = 2^{1552}$. The check of the full three-point identity then amounts to arithmetic on univariate polynomials whose coefficients are integers of several hundred thousand bits. The residual R is the certificate's own, and $\|R\|_1 \le \rho$ is checked exactly.

Packed sign tests on boxes. For the antiprism, the three-point separation inequality is recertified by new bisection covers. On each leaf box, ϕ is replaced by a Taylor minorant of degree 18, and a multiple $\mu\Delta$ with $\mu \ge 0$ is subtracted. A projective substitution then maps the box onto $[0,\infty)^3$, so that nonnegativity of all coefficients of the cleared polynomial proves the inequality. All coefficients are tested at once by one packed big-integer evaluation. The coefficients become base-2^k digits, a bound on the polynomial with absolute-value coefficients rules out carries, and a single bitwise test checks every sign.

Table 7 lists the measured costs of the most expensive kernel checks. The three-point identity for the prism is the largest single check; for the antiprism, most of the time goes to the separation covers.

10.6.2. *Differences from the proofs in this paper.* The formal proofs follow the steps of Procedure 2.1, but several steps are carried out in a form that is easier to check in the kernel.

- Nonnegativity of the Legendre sums S_k is derived from an exact addition identity in $\mathbb{Q}[u, v, t]$ and the positivity of the circle kernels, without spherical harmonics.
- The interpolation-gap estimate of Lemma 7.1 is replaced by Bernstein certificates for the gap inequality on finitely many cells.
- The classification of Section 8 is recomputed exhaustively in integer arithmetic, with cruder determinant perturbation radii.
- Strict local minimality is proved in Gram coordinates. Stationarity, convexity of the pair potential and the rank-three condition reduce it to a rational quadratic form in the C_N pair coordinates, which is certified positive definite. The alignment estimate and the Hessian bound of Section 9 are therefore not needed.
- For the antiprism, the three-point separation inequality is recertified by the covers described above. The separation polynomial is that of Proposition 5.3, rounded to an exact positive combination of kernels.

TABLE 7. Measured kernel checking times of the most expensive modules of the Lean formalization. A full build of the prism proof takes about 10 minutes on a 64-core machine.

Case	What the kernel checks	Time
Prism	Three-point identity, by the Kronecker zero test	∼6 min, 10 GB
Prism	Exhaustive labeling classification over $\mathbb{Z}$	∼75 s
Prism	Bernstein covers of the separation step	∼40 s
Prism	Scalar interpolation-gap cells	∼20 s
Prism	Positive definiteness of a 36-variable quadratic form	∼20 s
Prism	Each of the 14 weighted-square blocks	∼10 s
Antiprism	Three-point separation covers: 858 leaves in 221 modules	∼7 s per leaf
Antiprism	Exhaustive labeling classification over $\mathbb{Z}$	∼130 s
Antiprism	Three-point identity, by the Kronecker zero test	∼60 s
Antiprism	Positive semidefiniteness of a 45-variable quadratic form	∼55 s
Antiprism	Counting triangles through a pair	∼1–1.5 min, 9 GB
Antiprism	Scalar interpolation-gap cells	∼30 s

11. Concluding remarks

The usual symbolic-numeric route to an exact bound, rounding followed by projection onto the exact identity, needs slack that tight bounds with irrational optimal solutions do not have. Procedure 2.1 avoids the projection: the residual is kept, and only its coefficient norm is bounded. Exact optimality and uniqueness are then recovered from a coercivity estimate, from the rank constraint that the relaxation discards, and from local strong convexity modulo symmetry on a neighborhood larger than the proximity radius. Table 1 lists the constants linking these steps.

Scope. We expect the procedure to apply whenever a relaxation is numerically tight, its contact set together with the nonconvex constraints identifies the optimal solution up to symmetry, and the optimal solution is nondegenerate modulo symmetry. It does not apply directly when the relaxation has a positive duality gap, nor when the minimizer is degenerate.

What is generic and what is not. Several components do not depend on the instance: the positive kernels and their summation identities, the rounding with an explicit residual, the Hermite-remainder coercivity estimate (which needs only a positive lower bound for one high derivative of the pair potential), and the verification algorithms of Section 10, including the Kronecker zero test and the packed sign tests. Other components are specific to each instance. The two configurations require different domain reductions and contact conditions. The prism uses a scalar separation bound and six double Hermite contacts. The antiprism uses in addition a three-point separation bound, a contact at -1 and refined determinant bounds. Other numbers of points, or other potentials, would require new certificates and new geometric classifications.

Toward larger instances. The costs reported in Section 10 indicate where the procedure would become expensive. The three-point certificate grows with the degree needed for a nearly tight bound. The classification grows with the number of anchor types and with $|\mathcal{A}_N|^3$ descriptions per anchor. The local step grows with the $2N-3$ slice coordinates. Automating the search for the separation bound and the choice of the constants in Procedure 2.1 are natural next steps.

Declarations

Competing interests. The author declares no competing interests.

Funding. This research received no external funding.

Data availability. The certificates, the programs that verify them, and the Lean 4 formalizations of both theorems are openly available on Zenodo: for $N = 9$ at https://doi.org/10.5281/zenodo.23852043 [29], and for $N = 10$ at https://doi.org/10.5281/zenodo.23845065 [30].

Appendix A. Parameter and certificate data for the prism

The optimal radius is the unique zero in $(0, 1)$ of

$$F'(r) = -\frac{2\sqrt{3}}{r^2} + \frac{3r}{2(1-r^2)^{3/2}} + \frac{6r}{(4-r^2)^{3/2}} + \frac{6}{(2-r)^{3/2}} - \frac{6}{(2+2r)^{3/2}}.$$

It lies in $[k/10^{80}, (k+1)/10^{80}]$, where

```
k = 710548334092953811327704179272791243768034172409764397448884012404141629633136 90.
```

The signs of F' at the endpoints are established with 450-bit ball arithmetic. The bracket implies $1/2 < r_*^2 < 51/100$ and the bound $E_* < 644/25$ used in Section 5.

A.1. **The rational minorant and the certificate factors.** Let $m(t) = \sum_{i=0}^{15} c_i t^i$ be the rational polynomial of Proposition 6.2. With $M = (H_9 + \widehat{H}_9)/2$ and $s = 10^{-55}$, a 600-bit interval computation of the Hermite interpolants over the whole bracket shows

$$\sum_{i=0}^{15} \left| [t^i]M - c_i - s\,\mathbf{1}_{i=0} \right| < s; \tag{26}$$

in fact the left-hand side is about 1.505×10^{-70}. Therefore, for $|t| \le 1$, $M(t) - m(t) \ge s - \sum_i |[t^i]M - c_i - s\mathbf{1}_{i=0}| > 0$.

The rational energy bound in the identity is

$$U = \frac{2575998653126983156407570227376049402864191363647675944976214409505339 99}{10^{70}},$$

and $U > E_*$ holds uniformly over the bracket.

For each circle level k, the factor columns specify polynomials $p_{k,c}(x) = \sum_i f_{ki,c} L_i(x)$ with rational coefficients $f_{ki,c}$; their dimensions are given in Table 8. The kernels have total degree at most 20.

Table 8. The ten rational circle-kernel blocks for the prism.

k	0	1	2	3	4	5	6	7	8	9
Legendre coefficients per factor	11	10	9	8	7	6	5	4	3	2
Square factors	9	9	7	7	5	5	3	3	1	1

The weighted squares are expressed in the tensor Chebyshev basis

$$T_i(z(u))\,T_j(z(v))\,T_k(z(t)), \qquad z(x) = \frac{2000x + 433}{1567},$$

where z maps $[-1, 567/1000]$ onto $[-1, 1]$; Table 9 gives their numbers and degrees.

The residual R has total degree 20 and 1041 nonzero coefficients in the monomial basis. All coefficients of the certificate are given in [29].

Appendix B. Parameter and certificate data for the antiprism

Expanding (6) gives

$$\begin{aligned} F(a) = \frac{1}{2} &+ 4\sqrt{2}[(1-\sqrt{a})^{-1/2} + (1+\sqrt{a})^{-1/2}] + (4\sqrt{2}+2)(1-a)^{-1/2} \\ &+ 8[2-\sqrt{2}+(2+\sqrt{2})a]^{-1/2} + 8[2+\sqrt{2}+(2-\sqrt{2})a]^{-1/2}. \end{aligned} \tag{27}$$

TABLE 9. The 360 weighted squares for the prism, each symmetrized over the six permutations of (u, v, t).

Weight	Squares	Degree before squaring	Weighted degree
1	81	8	16
$1+u$	76	7	15
$b-u$	76	7	15
Δ	32	6	15
$(1+u)(b-u)$	76	7	16
$\Delta(1+u)(b-u)$	19	5	15

B.1. **The parameter bracket.** The optimal parameter lies in $[k/10^{70}, (k+1)/10^{70}]$, where

`k = 178664658444940490003165864676389710156095902738850943548528159541587 4`.

The signs of F' at the two endpoints, established by interval arithmetic, enclose its unique zero in this interval. All energy comparisons and interpolation enclosures use this bracket.

B.2. **The rational minorant and the certificate factors.** The rational energy bound in Proposition 6.2 is

$$U = \frac{654338989202951763091141150393998800594106829970060712992 6819}{200000000000000000000000000000000000000000000000000000000000000000000000}.$$

The inequalities $m \le M$ and $U > E_*$ hold uniformly over the bracket. More precisely, with $s = 10^{-59}$ and $m(t) = \sum_j c_j t^j$, validated interpolation shows

$$\sum_{j=0}^{16} \left| [t^j]M - c_j - s\,\mathbf{1}_{j=0} \right| < s, \tag{28}$$

which gives $m(t) \le M(t)$ for $|t| \le 1$.

Each kernel factor is a polynomial $p_{k\ell}(x) = \sum_i f_{ki\ell} L_i(x)$ with rational coefficients; Table 10 gives the dimensions. The Legendre part uses L_1 and L_3 with nonnegative rational coefficients. The kernels have total degree at most 20, and the nonzero circle levels are $k = 0, \dots, 9$.

TABLE 10. The ten rational circle-kernel blocks for the antiprism. The block $k = 10$ is zero.

k	0	1	2	3	4	5	6	7	8	9
Legendre coefficients per factor	11	10	9	8	7	6	5	4	3	2
Square factors	9	9	8	7	5	5	4	3	1	1

The polynomial W_{10} is the symmetrization of the 336 weighted squares in Table 11. The squares are expressed in the tensor Chebyshev basis in $z(x) = (100x + 27)/73$, an affine map of $[-1, b]$ onto $[-1, 1]$; this basis serves only to represent coefficients.

The residual R has total degree 20, 1041 nonzero coefficients and $\rho \approx 8.009784771683718 \times 10^{-59}$. All coefficients of the certificate are given in [30].

APPENDIX C. THE ALIGNMENT ESTIMATE

We prove Lemma 9.1. All matrix norms are operator norms induced by the Euclidean norm.

For the prism, take the candidate anchors p_0, p_1, p_2, the vertices of the upper triangle. Their Gram matrix has constant off-diagonal entry $g = 1 - 3r_*^2/2$. Since $1/2 < r_*^2 < 51/100$, we have $0 < g < 1/4$, and the eigenvalues $1 - g, 1 - g, 1 + 2g$ exceed $3/4$. For the antiprism, take the

TABLE 11. The 336 weighted squares for the antiprism, each symmetrized over the six permutations of (u, v, t).

Weight	Squares	Degree before squaring	Weighted degree
1	77	8	16
$1+u$	71	7	15
$b-u$	69	7	15
Δ	31	6	15
$(1+u)(b-u)$	71	7	16
$\Delta(1+u)(b-u)$	17	5	15

north pole and the first two vertices of the upper square, p_0, p_2, p_3. Their Gram determinant is $(1-a_*)^2 > 16/25$ and the trace is 3; the product of the two largest eigenvalues is at most $9/4$, so the least eigenvalue exceeds $64/225 > 1/4$.

Let P and X be the 3×3 matrices whose columns are the candidate and actual anchors, with Gram matrices $A_* = P^T P$ and $A = X^T X$. Their off-diagonal entries differ by less than d, so $\|A - A_*\| < 2d$, and in both cases the eigenvalue margin gives $\lambda_{\min}(A) > 1/4$ for $d \le 10^{-9}$. The polar decompositions $P = UA_*^{1/2}$ and $X = VA^{1/2}$ yield the orthogonal alignment UV^T.

To bound the error of the aligned anchors, note that for positive definite S, T,

$$S(S-T) + (S-T)T = S^2 - T^2, \qquad S - T = \int_0^\infty e^{-tS}(S^2 - T^2)e^{-tT}\, dt,$$

and consequently

$$\|S - T\| \le \frac{\|S^2 - T^2\|}{\lambda_{\min}(S) + \lambda_{\min}(T)}.$$

Applied to the square roots of the two Gram matrices, whose least eigenvalues sum to more than one, this shows that the aligned anchors differ by less than $2d$. For corresponding points x, p, the vectors of anchor inner products differ by less than $\sqrt{3}d$, and hence

$$\|P^T(x-p)\| \le \|P - X\|\|x\| + \|X^T x - P^T p\| < (2+\sqrt{3})d.$$

Since $\|(P^T)^{-1}\| < 2$, we obtain $\|x - p\| < 2(2+\sqrt{3})d < 8d$.

A minimal rotation carrying point 0 to p_0 differs from the identity by the chord distance between them, so all point errors become less than $16d$. Project the second point and its candidate onto $p_0^\perp$; the projections differ by less than $16d$. The candidate projection has length $\sqrt{1-g^2} > 4/5$ for the prism and $\sqrt{1-a_*} > 4/5$ for the antiprism. Since

$$\Big\| \frac{a}{\|a\|} - \frac{b}{\|b\|} \Big\| \le \frac{2\|a-b\|}{\|b\|},$$

the rotation about p_0 that aligns the projection with the candidate direction is within $40d$ of the identity. It fixes point 0, and all point errors are now less than $56d$.

For each point, $p_i \cdot x_i = 1 - \|x_i - p_i\|^2/2 > 1/2$, so the inverse chart in (24) gives $\|q_i\| < 112d < 128d$. Both coordinates of point 0 vanish. For the prism, point 1 lies in the plane spanned by p_0 and p_1, so its component along $(p_0 \times p_1)/\|p_0 \times p_1\|$ vanishes; for the antiprism, the second point has the correct azimuth, so its azimuthal coordinate vanishes. Positivity of the aligned projections selects the correct branches. These are exactly the three fixed coordinates of Section 9.

APPENDIX D. FRAMES AND THE LOCAL HESSIAN

For a triangle or square vertex $(r\cos\theta, r\sin\theta, z)$ we use the orthonormal tangent frame

$$b_1 = (-\sin\theta, \cos\theta, 0), \qquad b_2 = (-z\cos\theta, -z\sin\theta, r).$$

At a cap of the prism we use the azimuthal and vertical unit vectors. At point 1 of the prism the frame is replaced by $(u, p_1 \times u)$ with $u = (p_0 \times p_1)/\|p_0 \times p_1\|$, and at the poles of the antiprism we use (e_1, e_2). These frames are orthonormal for every value of the parameter in the bracket.

For a single chart write $w = p + Bq$ and $s = \sqrt{1 + \|q\|^2}$. The first and second derivatives of the chart are

$$J_b = B_b/s - wq_b/s^3,$$
$$K_{bc} = (-B_b q_c - B_c q_b - w\mathbf{1}_{b=c})/s^3 + 3wq_b q_c/s^5.$$

For a difference $v = x_i - x_j$, the ambient Hessian of $\|x_i - x_j\|^{-1}$ with respect to x_i is

$$\frac{3vv^T}{\|v\|^5} - \frac{I}{\|v\|^3}.$$

The Hessian in local coordinates is obtained by pulling back with the Jacobians and adding the ambient gradient contracted with K_{bc}; the latter terms are essential for the constrained second derivative.

All terms are enclosed simultaneously over the parameter bracket and the coordinate box. After removal of the fixed coordinates, an interval LDL^T elimination of $D^2E_N - I/1000$ yields strictly positive lower bounds for all pivots. Hence every matrix in the enclosure has positive pivots and is positive definite. For the prism the box has 15 coordinates and radius 10^{-7}, and the computation uses 450-bit outward dyadic arithmetic; for the antiprism the box has 17 coordinates and radius 10^{-6}, and the computation uses the lattice $2^{-320}\mathbb{Z}$. Quotients and square roots are rounded outward.

Appendix E. The addition theorem

We record the form of the addition theorem used in Section 4. A homogeneous polynomial on $\mathbb{R}^3$ is *harmonic* if its Laplacian vanishes. Let $Y_1, \dots, Y_{2j+1}$ be a real orthonormal basis of the restrictions to $\mathbb{S}^2$ of the harmonic polynomials of degree j, with respect to the normalized inner product $(4\pi)^{-1}\int_{\mathbb{S}^2} fg\,dS$. The addition theorem states

$$L_j(x \cdot y) = \frac{1}{2j+1}\sum_{m=1}^{2j+1} Y_m(x)Y_m(y).$$

Summing over a finite set of points gives

$$\sum_{i,l} L_j(x_i \cdot x_l) = \frac{1}{2j+1}\sum_{m=1}^{2j+1}\Big(\sum_i Y_m(x_i)\Big)^2 \geq 0,$$

which is the two-point analogue of (10).

For $j = 1$ one may take Y_m to be $\sqrt{3}$ times the coordinate functions, and the formula reduces to $\sum_{i,l} x_i \cdot x_l = \|\sum_i x_i\|^2$. For $j = 2$, with $M = \sum_i x_i x_i^T$ and N points,

$$\sum_{i,l} L_2(x_i \cdot x_l) = \frac{3}{2}\operatorname{tr}(M^2) - \frac{N^2}{2},$$

because $\sum_{i,l}(x_i \cdot x_l)^2 = \operatorname{tr}(M^2)$. If $\lambda_1, \lambda_2, \lambda_3$ are the eigenvalues of M, then $\sum \lambda_i = N$ and $\sum \lambda_i^2 \geq N^2/3$, which gives nonnegativity directly in this case. Section 8 uses a quantitative form of this calculation.

References

1. N. N. Andreev, *An extremal property of the icosahedron*, East Journal on Approximations **2** (1996), no. 4, 459–462.
2. Christine Bachoc and Frank Vallentin, *New upper bounds for kissing numbers from semidefinite programming*, Journal of the American Mathematical Society **21** (2008), no. 3, 909–924, https://arxiv.org/abs/math/0608426.
3. Henry Cohn and Abhinav Kumar, *Universally optimal distribution of points on spheres*, Journal of the American Mathematical Society **20** (2007), no. 1, 99–148, https://arxiv.org/abs/math/0607446.
4. Henry Cohn and Jeechul Woo, *Three-point bounds for energy minimization*, Journal of the American Mathematical Society **25** (2012), no. 4, 929–958, https://arxiv.org/abs/1103.0485.
5. David de Laat, *Moment methods in energy minimization: new bounds for Riesz minimal energy problems*, Transactions of the American Mathematical Society **373** (2020), no. 2, 1407–1453, https://arxiv.org/abs/1610.04905.
6. Leonardo de Moura and Sebastian Ullrich, *The Lean 4 theorem prover and programming language*, Automated Deduction – CADE 28, Lecture Notes in Comput. Sci., vol. 12699, Springer, 2021, pp. 625–635.
7. P. Delsarte, J. M. Goethals, and J. J. Seidel, *Spherical codes and designs*, Geometriae Dedicata **6** (1977), no. 3, 363–388, https://doi.org/10.1007/BF03187604.
8. Rida T. Farouki, *The Bernstein polynomial basis: a centennial retrospective*, Computer Aided Geometric Design **29** (2012), no. 6, 379–419, https://doi.org/10.1016/j.cagd.2012.03.001.
9. Thomas Hales, Mark Adams, Gertrud Bauer, Tat Dat Dang, John Harrison, Le Truong Hoang, Cezary Kaliszyk, Victor Magron, Sean McLaughlin, Tat Thang Nguyen, Quang Truong Nguyen, Tobias Nipkow, Steven Obua, Joseph Pleso, Jason Rute, Alexey Solovyev, Thi Hoai An Ta, Nam Trung Tran, Thi Diep Trieu, Josef Urban, Ky Vu, and Roland Zumkeller, *A formal proof of the Kepler conjecture*, Forum of Mathematics, Pi **5** (2017), e2, https://doi.org/10.1017/fmp.2017.1.
10. John Harrison, *Verifying nonlinear real formulas via sums of squares*, Theorem Proving in Higher Order Logics (TPHOLs 2007), Lecture Notes in Comput. Sci., vol. 4732, Springer, 2007, pp. 102–118.
11. David Harvey, *Faster polynomial multiplication via multipoint Kronecker substitution*, Journal of Symbolic Computation **44** (2009), no. 10, 1502–1510, https://arxiv.org/abs/0712.4046.
12. Fredrik Johansson, *Arb: efficient arbitrary-precision midpoint-radius interval arithmetic*, IEEE Transactions on Computers **66** (2017), no. 8, 1281–1292, https://arxiv.org/abs/1611.02831.
13. Erich Kaltofen, Bin Li, Zhengfeng Yang, and Lihong Zhi, *Exact certification of global optimality of approximate factorizations via rationalizing sums-of-squares with floating point scalars*, Proceedings of the 2008 International Symposium on Symbolic and Algebraic Computation (ISSAC '08), ACM, 2008, https://doi.org/10.1145/1390768.1390792, pp. 155–164.
14. Liudmyla Kryvonos, Lukas Liehr, and Mitchell A. Taylor, *Energy minimization for eight points on the sphere*, arXiv:2609.22077, 2026, https://arxiv.org/abs/2609.22077.
15. Jean B. Lasserre, *Global optimization with polynomials and the problem of moments*, SIAM Journal on Optimization **11** (2001), no. 3, 796–817, https://doi.org/10.1137/S1052623400366802.
16. Victor Magron and Mohab Safey El Din, *On exact Reznick, Hilbert–Artin and Putinar's representations*, Preprint, arXiv:1811.10062, 2018, https://arxiv.org/abs/1811.10062.
17. César Muñoz and Anthony Narkawicz, *Formalization of Bernstein polynomials and applications to global optimization*, Journal of Automated Reasoning **51** (2013), 151–196, https://doi.org/10.1007/s10817-012-9256-3.
18. Arnold Neumaier, *Complete search in continuous global optimization and constraint satisfaction*, Acta Numerica **13** (2004), 271–369, https://doi.org/10.1017/S0962492904000194.
19. Pablo A. Parrilo, *Semidefinite programming relaxations for semialgebraic problems*, Mathematical Programming **96** (2003), no. 2, 293–320, https://doi.org/10.1007/s10107-003-0387-5.
20. Helfried Peyrl and Pablo A. Parrilo, *Computing sum of squares decompositions with rational coefficients*, Theoretical Computer Science **409** (2008), no. 2, 269–281, https://doi.org/10.1016/j.tcs.2008.09.025.
21. Richard Evan Schwartz, *The five-electron case of Thomson's problem*, Experimental Mathematics **22** (2013), no. 2, 157–186, https://arxiv.org/abs/1001.3702.
22. The mathlib Community, *The Lean mathematical library*, Proceedings of the 9th ACM SIGPLAN International Conference on Certified Programs and Proofs (CPP 2020), ACM, 2020, pp. 367–381.
23. J. J. Thomson, *On the structure of the atom: an investigation of the stability and periods of oscillation of a number of corpuscles arranged at equal intervals around the circumference of a circle; with application of the results to the theory of atomic structure*, The London, Edinburgh, and Dublin Philosophical Magazine and Journal of Science **7** (1904), no. 39, 237–265, https://doi.org/10.1080/14786440409463107.
24. *Thomson problem, $N = 7$: Lean proof package*, Proof package, version of 27 September 2026, 2026, https://github.com/huwngtran/thomson-n7-lean. Accessed 2 November 2026.

25. Joseph Tooby-Smith and Alex Zughaid, *Thomson-N-8-Warrant: formalizing the $N = 8$ solution to the Thomson problem*, Lean formalization, 2026, https://github.com/jstoobysmith/Thomson-N-8-Warrant. Accessed 2 November 2026.
26. Joachim von zur Gathen and Jürgen Gerhard, *Modern computer algebra*, third ed., Cambridge University Press, Cambridge, 2013.
27. David J. Wales and Jonathan P. K. Doye, *Global optimization by basin-hopping and the lowest energy structures of Lennard-Jones clusters containing up to 110 atoms*, The Journal of Physical Chemistry A **101** (1997), no. 28, 5111–5116, https://doi.org/10.1021/jp970984n.
28. David J. Wales and Sidika Ulker, *Structure and dynamics of spherical crystals characterized for the Thomson problem*, Physical Review B **74** (2006), no. 21, 212101, https://doi.org/10.1103/PhysRevB.74.212101.
29. Katherine Xie, *Optimality and uniqueness in the nine-electron Thomson problem: verification code and certificates*, Zenodo, 2026, https://doi.org/10.5281/zenodo.23852043.
30. ———, *Optimality and uniqueness in the ten-electron Thomson problem: verification code and certificates*, Zenodo, 2026, https://doi.org/10.5281/zenodo.23845065.
31. V. A. Yudin, *Minimum potential energy of a point system of charges*, Diskretnaya Matematika **4** (1992), no. 2, 115–121, In Russian; English translation in Discrete Mathematics and Applications 3 (1993), no. 1, 75–81. https://doi.org/10.1515/dma.1993.3.1.75.

University of California, Irvine
Email address: kathex5@uci.edu